Evolution of Microstructure in Brazed Joints of Austenitic-Martensitic Stainless Steel with Pure Silver Obtained with Ag-27Cu-5Sn Brazing Filler Material

S. GANGADHARAN, D. SIVAKUMAR, T. VENKATESWARAN, and KAUSTUBH KULKARNI

Brazing of an austenitic-martensitic stainless steel (AMSS) with pure silver was carried out at 1053 K, 1073 K, and 1093 K (780 °C, 800 °C, and 820 °C) with Ag-27Cu-5Sn (wt pct) as brazing filler material (BFM). Wettability of the liquid BFM over base AMSS surface was found to be poor. Application of nickel coating to the steel was observed to enhance the wettability and to enable the formation of a good bond between BFM and the steel. The mechanism responsible for enhanced metallurgical bonding of the BFM with AMSS in the presence of nickel coating was explained based on diffusional interactions and uphill diffusion of iron, chromium and nickel observed in the brazed microstructure. Good diffusion-assisted zone was observed to form on silver side at all three temperatures. Four phases were encountered within the joint including silver solid solution, copper solid solution, Cu_3Sn intermetallic and Ni-Fe solid solution. The Cu_3Sn intermetallic was present in small amounts in the joints brazed at 1053 K and 1073 K (780 °C and 800 °C). The joint formed at 1093 K (820 °C) exhibited the absence of Cu_3Sn, fewer defects and larger diffusion-assisted zone. Hardness of base AMSS was found to reduce during brazing due to austenite reversion and post-brazing sub-zero treatment for 2.5 hours was found suitable to recover the hardness.

DOI: 10.1007/s11661-016-3787-x

I. INTRODUCTION

JOINING of silver to stainless steel is required in manufacturing of many components of aerospace vehicles such as in rotating parts of a turbo pump where good tribological properties are required. In such applications, stainless steel, having a good combination of corrosion resistance and strength[1] is used for structural applications, whereas pure silver, due to its good friction properties and high thermal conductivity, is used for preventing the excessive heating due to friction.[2–4] Joining of silver to steel is critical since it usually produces a poor joint. For example, Atasoy *et al.*[5] reported the propagation of crack at the interface between silver interlayer and low carbon steel, whereas Deng *et al.*[6] reported propagation of fracture through silver interlayer in their respective work of diffusion bonding of Ti and steels with silver as an interlayer. The poor bond between steel and silver is mainly on account of the highly positive heat of mixing between silver and iron and their poor solubility into each other as observed from the Fe-Ag binary phase diagram.[7] In addition, if high temperatures are used during the joining of these dissimilar metals, it may end up deteriorating the properties of structural steels such as austenitic-martensitic steels, which are given special heat treatments for establishing their desired properties. Hence, there is a need to develop a brazing process that would yield a strong and reliable joint without affecting the properties of the base material. Ag-Cu based alloys[8–10] are good candidates for a brazing filler material because of the presence of lower melting eutectic in this system and their compatibility with silver.[11,12] Tin is usually added in commercial Ag-Cu based filler alloys to further lower the melting temperature of the alloy and to improve the spreadability of the filler metal.[10] However, Ag-Cu-Sn ternary system contains a variety of intermetallic phases, which are brittle. Hence, the presence of intermetallics in the brazed joint may yield joints with poor strength. Thus, studying the evolution of microstructure in the brazed joints between austenitic-martensitic stainless steel and silver obtained with Ag-Cu-Sn-based brazing filler material is one of the motivations for this work.

An austenitic-martensitic class stainless steel (AMSS) is a good material for cryogenic application[13] hence it

S. GANGADHARAN, formerly Master's Student with the Department of Materials Science and Engineering, Indian Institute of Technology Kanpur, U.P. 208016, India, is now Manager with Tata Steel Ltd., Jamshedpur, India. D. SIVAKUMAR, Scientist SG, and T. VENKATESWARAN, Scientist SE, are with the Materials Processing and Research Group, Vikram Sarabhai Space Center, ISRO, Trivandrum, India. KAUSTUBH KULKARNI, Assistant Professor, is with the Department of Materials Science and Engineering, Indian Institute of Technology Kanpur. Contact e-mail: kkaustub@iitk.ac.in.

Manuscript submitted February 20, 2016.
Article published online October 5, 2016

was used as one of the base materials in this study. An important feature of this steel is that its properties can be modified over a wide range by heat treatments and cold working.[13,14] To achieve the desired strength, this AMSS has to be given a particular heat treatment,[1,15,16] for example, austenitization at 1263 K (990 °C) followed by air or fast cooling, sub-zero treatment at 203 K (−70 °C) for 2 hours and tempering at 673 K (400 °C) for 1 hour. The high temperatures encountered during the brazing process may deteriorate the microstructure and properties of the AMSS due to reversion of austenite.[17,18] Therefore, studying the effect of brazing treatment on the base materials is also a crucial part of this study. Thus, the objectives of the present study were to assess the effect of brazing on the AMSS properties using simulated brazing cycle, to assess the effect of brazing temperature on the evolution of microstructure in brazed joint of AMSS and pure silver obtained with a Ag-Cu-Sn braze foil, and to optimize the brazing process based on the microstructure and properties obtained in and across the brazed joint.

II. EXPERIMENTAL WORK

In this study, brazing of the AMSS with pure silver was carried out with 68Ag-27Cu-5Sn (wt pct) that is used as a Brazing Filler Material (BFM). Table I presents the composition of the base AMSS steel as measured by optical emission spectroscopy (OES). Differential Scanning Calorimetry (DSC) was performed on BFM using NETZSCH STA 449 F3 at the heating rates of 5 K/min, 10 K/min, and 20 K/min (5 °C/min, 10 °C/min, and 20 °C/min) in Ar atmosphere to determine its liquidus temperature. Prior to the experiment, with identical experimental conditions and parameters (such as heating rate, temperature, atmosphere, crucible etc.), a zero line correction was carried out to obtain highly accurate results without any asymmetry. In order to assess the effect of brazing conditions on the base AMSS, simulated brazing cycles were conducted on the AMSS at five different brazing temperatures including 1053 K, 1073 K, 1093 K, 1123 K, and 1173 K (780 °C, 800 °C, 820 °C, 850 °C, and 900 °C) for 15 minutes. Heat treatment cycle employed during simulated brazing cycle was similar to the heating sequence to be employed during actual brazing process [as shown in Figure 1(b)] with two additional temperatures than actual brazing. The cycle consisted of two isothermal holdings, one at 873 K (600 °C) and another one at the brazing temperature of 1053 K, 1073 K, 1093 K, 1123 K, or 1173 K (780 °C, 800 °C, 820 °C, 850 °C, or 90 0°C), followed by air cooling for the simulated brazing cycles. The simulated brazing cycles were conducted in a muffle furnace and the observed heating rate was approximately 10 K/min (10 °C/min). The steel samples subjected to simulated brazing cycles were sectioned and metallographically prepared for microstructure characterization. Ferritescopy was used to determine the fraction of martensite in AMSS subjected to simulated brazing cycles. Ferritescopy, which measures the fraction of a magnetic phase present (ferrite or martensite) in a steel based on magnetic susceptibility of the steel sample, was used for measurement of martensite fraction in the base AMSS samples. The instrument was calibrated with multiple samples of known ferrite content ranging from 0.2 to 40 pct. Since the steel used in this study is austenitic stainless steel type and only martensite can be obtained with sub-zero treatment, ferrite fraction can be safely assumed to be negligible. This assumption should not affect the results as we were interested in only relative measurements of martensite in the simulated brazing samples treated at various temperatures. Minimum 10 readings were taken on each sample.

Brazing was carried out in a vacuum furnace by making lap joints between two AMSS strips or between AMSS and pure silver as shown by the schematic in Figure 1(a). A 0.3 mm-thick BFM foil was sandwiched between the two base metals and a 200 g molybdenum dead weight was used to ensure good contacts during brazing. Molybdenum was used for weight mainly because of its high density and stability at elevated temperature due to its very high melting point. The brazing assembly was placed in a vacuum brazing furnace evacuated to 10^{-4} mbar. The temperature was then raised to 873 K (600°C) at a rate of 10 K/min (10 °C/min) and held there for 15 minutes. The temperature was then further raised to the desired brazing temperature at a rate of 10 K/min (10 °C/min) and the brazing assembly was held at the brazing temperature for 15 minutes. At the end of the brazing cycle, the sample was cooled by 1 bar gas quenching. The schematic brazing cycle is presented in Figure 1(b). Initially, brazing was carried out with bare AMSS at two different temperatures [1058 K and 1093 K (785 °C and 820 °C)] and AMSS/pure silver braze joints were fabricated to examine the wetting behavior of BFM over the base materials. Since wetting of AMSS with BFM was found to be poor, further brazing was conducted with the steel coated with nickel. The nickel coating was applied to AMSS by using standard Wood's nickel bath composed of a mixture of nickel chloride solution (240 g/L) and hydrochloric acid (250 mL/L) with electrical current density of 12 A/dm^2. The electroplating was carried out at room temperature for two minutes. Before application of nickel coating, AMSS surface was cleaned by degreasing with trichloroethylene, pickling with 30 pct HCl and activation using 10 pct H_2SO_4 bath. The surface was rinsed in running water each time after degreasing and pickling and was double rinsed in running water after activation. Brazing of nickel-coated steel with silver was conducted at 1053 K, 1073 K and 1093 K (780 °C, 800 °C and 820 °C) using the process explained earlier. The brazed samples were then sectioned into two halves. One half was used to examine the microstructure and microhardness properties developed in the brazed joints. Second half was given sub-zero treatment in liquid nitrogen at about 203 K (−70 °C) for 0.5 and 2.5 hours and was further examined for changes in hardness of the base AMSS. Separate braze joints were also prepared for estimation of lap shear strength of the braze joint. Testing of lap shear strength of the joints of AMSS to pure silver and of AMSS to AMSS was performed as per the standard AWS C3.2.

Table I. Composition of AMSS Stainless Steel as Measured by OES

Element	C	Cr	Ni	Mn	Si	Al	P	S	Fe
Wt pct	0.07	16.5	6.6	0.41	0.39	0.014	0.013	0.009	balance

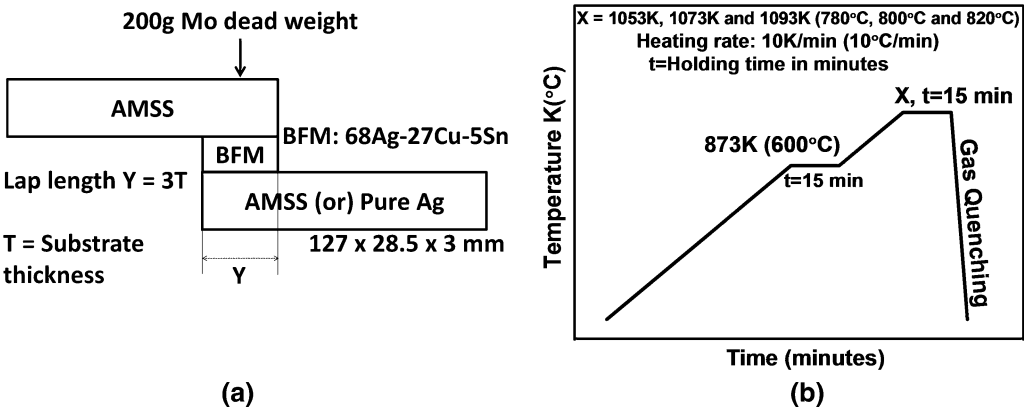

Fig. 1—(*a*) Schematic of the lap shear joint configuration prepared by brazing and (*b*) brazing cycle adapted in this study.

Metallographically prepared samples were etched using Acetic Glyceregia (mixture of 15cc HCl, 10cc HNO_3, 10cc CH_3COOH and two to three drops of glycerine) for 1 second. Scanning Electron Microscope (SEM) images were captured in Back Scattered Electron (BSE) mode with JEOL JSM 6010LA SEM equipped with EDS analyzer. The elemental analysis was carried out with an Energy-Dispersive Spectroscope (EDS) using accelerating voltage of 20 kV and probe current of 350 pA. Quantitative elemental analysis was also carried out across the brazed joints using JEOL JXA-8230 Electron Probe Micro-Analyzer (EPMA) with accelerating voltage of 20 kV, beam current of 20nA and beam diameter of less than 1μm in Wave-length-Dispersive Spectroscopy (WDS) mode. The pure elemental standards of iron, nickel, chromium, silver, copper, and tin were used for the EPMA analysis. Variation of the microhardness across the brazed joint was studied using Vickers microhardness tester with a load of 1 N applied for 10 seconds.

X-ray diffraction (XRD) patterns were collected with Bruker D8 Focus diffractometer with Cu-Kα radiation using a step size of 0.02 deg and a scan speed of 0.4 second/step. In order to obtain maximum exposure of the brazed area to X-rays during XRD analysis, separate specimens were prepared by taking sections of the brazed joints at a slanting angle to the interface plane.

III. RESULTS AND DISCUSSION

A. *Deciding the Brazing Temperature Range*

Figure 2 shows the DSC curves of BFM obtained at the heating rates of 5 K/min, 10 K/min, and 20 K/min (5 °C/min, 10 °C/min, and 20 °C/min). The obvious endothermic peaks are observed at 1021.4 K, 1023.3 K, and 1026.1 K (748.4 °C, 750.3 °C, and 753.1 °C) for the

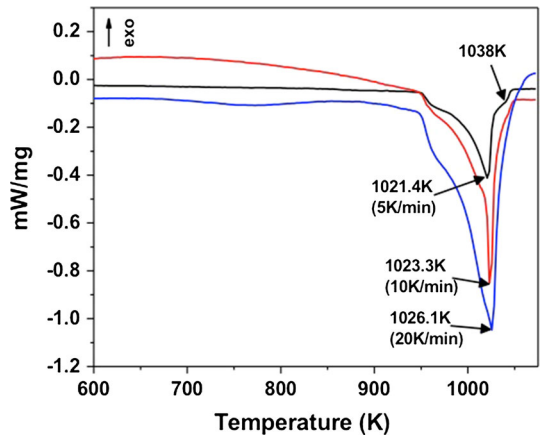

Fig. 2—DSC curves of BFM obtained at heating rates of 5 K/min, 10 K/min, and 20 K/min (5 °C/min, 10 °C/min, and 20 °C/min).

samples studied at heating rates of 5 K/min, 10 K/min, and 20 K/min (5 °C/min, 10 °C/min, and 20 °C/min), respectively. However, a second melting event is also observed at about 1038 K (765 °C) at the slower heating rate of 5 K/min. Thus, the minimum possible brazing temperature should be above 1038 K (765 °C). Another parameter which is important in deciding the brazing temperature is the flowability of the liquid BFM at the brazing temperature. Thus, the minimum temperature for brazing was fixed at 1053 K (780 °C), at which the liquid BFM was seen to have good enough flowability. At very high temperatures, the liquid may tend to ooze out of the joint due to very low viscosity. Thus, the brazing experiments were carried out in the temperature range from 1053 K to 1093 K (780 °C to 820 °C).

B. *Simulated Brazing Cycles*

One of the base materials, AMSS, is composed of two phases *viz*. austenite and martensite. The measured M_s

(martensitic start) temperature for the AMSS is 310 K (37 °C). Hence, after the initial heat treatment of AMSS at 1263 K (990 °C), the steel has only small amount of martensite in the range from 10 to 20 pct at room temperature. After exposing to the sub-zero treatment at 203 K (−70 °C), some austenite converts to martensite by martensitic transformation. The parameters of the martensitic transformation and quantity of martensite obtained in these steels can be controlled by the composition and heat treatment employed.

During brazing, properties of AMSS can be affected due to transformation of martensite. To assess the potential changes in properties, simulated brazing cycles were conducted on the AMSS. Figures 3(a) through (f) present the SEM micrographs of AMSS before and after simulated brazing cycles at the five temperatures studied. From the base AMSS micrograph (Figure 3(a)), two phases can be seen *viz*. martensite needles and austenite. During the high-temperature exposure, as shown in Figures 3(b) through (f), martensite needles started transforming into austenite phase. Reduction in length of the martensite needles that occurred during brazing is clearly evident from the microstructures shown in Figures 3(b) through (f). Variations in martensite phase fraction and hardness of the AMSS base material after simulated brazing at various temperatures are presented in Figures 4(a) and (b). Martensite phase fractions were determined using ferritescopy. The reduction in martensite phase fraction at the brazing temperatures was confirmed by the ferritoscope analysis as presented in Figure 4(a). It can also be seen from Figure 4(b) that the hardness of the base material reduced considerably after simulated brazing cycle at all temperatures. However, it can be observed that there was not much variation in hardness with brazing temperature within the range from 1053 K to 1123 K (780 °C to 900 °C). This reduction in hardness upon brazing may be attributed to the dissolution of martensite at higher brazing temperatures resulting in the reduction of its phase fraction after simulated brazing cycle. From the observations of simulated brazing cycles, it can be said that brazing temperature can be fixed between 1053 K and 1123 K (780 °C and 900 °C). However, considering the excessive flowability of the liquid filler metal at higher temperatures, brazing temperatures were fixed as 1053 K, 1073 K, and 1093 K (780 °C, 800 °C, and 820 °C). The simulated brazing cycles also suggested that post-brazing sub-zero treatment may be required for recovering the properties of the base material.

C. *Brazing with AMSS Without Nickel Coating*

Initially, brazing was carried out to obtain the joints of AMSS to AMSS and AMSS to pure silver using 68Ag-27Cu-5Sn BFM foil. Both the base metals were prepared only for the desired surface roughness and no other preparation such as an intermediate coating was done. Thus, the BFM was directly in contact with the steel. Figures 5(a) through (d) show the various micrographs of the brazed samples. Figures 5(a) and (b) show the AMSS/AMSS joints which were brazed at 1058 K and 1093 K (785 °C and 820 °C), respectively, whereas Figures 5(c) and (d) present the micrographs of the brazed joints of AMSS/pure silver which were brazed at 1058 K and 1093 K (785 °C and 820 °C), respectively. These microstructures clearly show the presence of gaps or voids between AMSS and BFM. Especially in Figure 5(a), the spherical shape of BFM formed over the surface of AMSS clearly highlights the poor wettability of the BFM on the AMSS. These spherical solidified particles suggested that the contact angle between liquid BFM droplet and AMSS surface was high, which led to poor wettability of the BFM over the bare surface of AMSS. In order to produce a well-brazed joint, the wetting issue needs to be addressed. The poor wetting of liquid BFM on stainless steel has been attributed to the presence of Cr_2O_3 layer on the steel.[13] Another possible reason for poor bond observed between the steel and BFM is the high positive enthalpy of mixing between iron and silver, and resulting poor solubility of the two elements into each other.[19,20] According to Kozlova *et al*.,[21] this problem can be resolved by employing the brazing temperatures beyond 1133 K (860 °C) for stainless steel because of the dissociation of Cr_2O_3. However, beyond 1133 K (860 °C), fluidity of liquid BFM would be very high and it tends to ooze out of the joint. Another commonly used method for improving the wettability of liquid BFM is to form a layer of a compatible metal over base metal surface.[22,23] Usually, nickel and copper have been suggested for this purpose. However, heat of mixing (ΔH^{mix}) of copper and iron is positive,[24] whereas that of nickel and iron is negative.[25] Hence, nickel coating was decided to be deposited over AMSS surface before joining. Hosking *et al*.[26] have used nickel coating on duplex stainless steel to overcome the wetting issue of filler metal over the stainless steel. It can be observed from Figures 5(c) and (d) that the joint on the silver side exhibited good metallurgical bonding and no wettability problem would be anticipated on silver side during brazing.

D. *Brazing with Nickel Coating on AMSS*

1. *Microstructure Analysis*

Further brazing was carried out at three different brazing temperatures *i.e.,* 1053 K, 1073 K, and 1093 K (780 °C, 800 °C, and 820 °C) using AMSS electroplated with nickel coating. Figures 6(a) through (f) show the microstructures of brazed joints obtained between nickel-coated AMSS and pure silver at all brazing temperatures. The microstructure can be divided into four distinct regions, which are identified as AMSS, interface, brazing filler material (BFM), and pure silver as labeled in the micrographs.

As shown in Figures 6(a) through (f), very good metallurgical bonding was observed near both the interfaces. A sharp physical interface is clearly evident on the steel side of the joint, which is delineated by dark second phase particles. The fraction of second phase particles seems to decrease going from the steel side to the silver side of the joint. The interface on the silver side

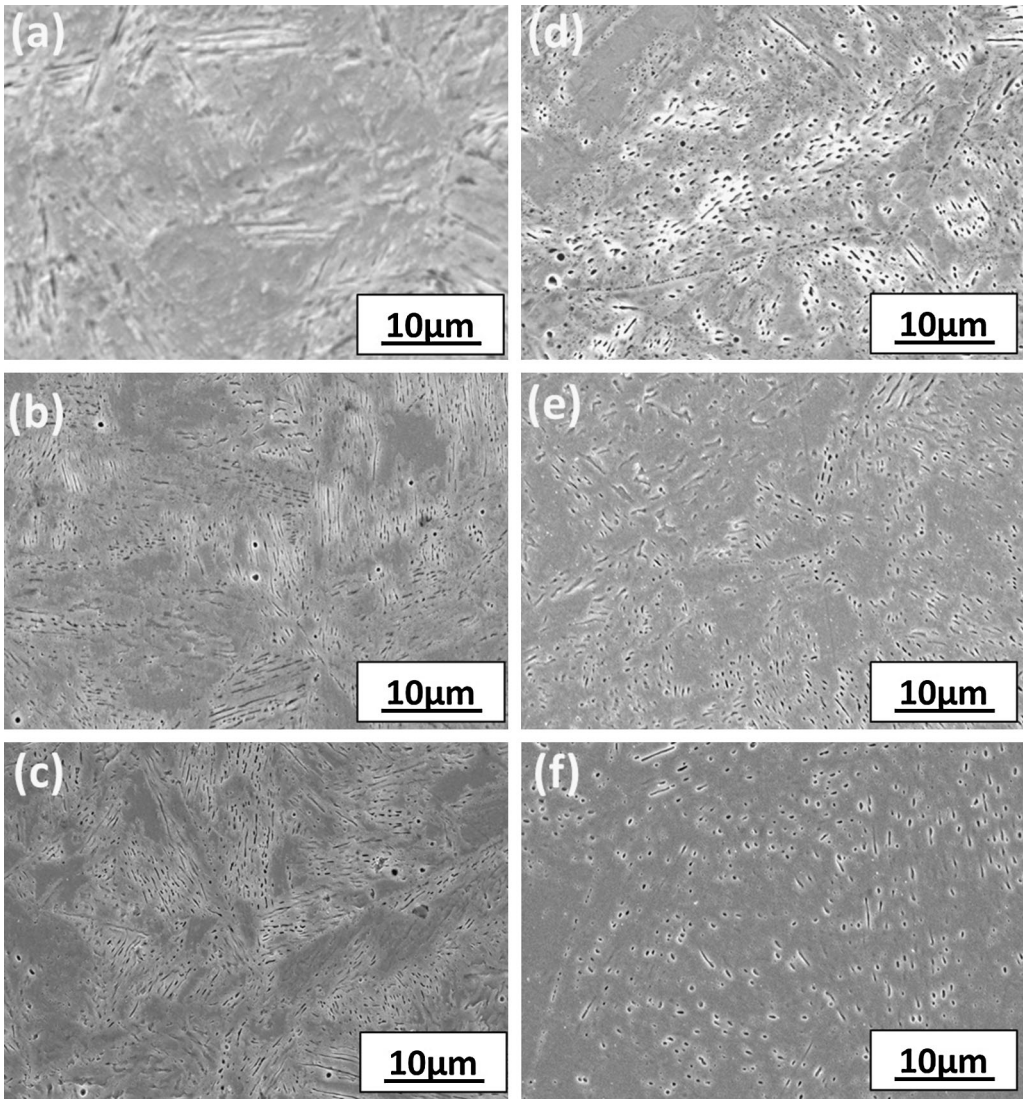

Fig. 3—SEM micrographs of (*a*) base AMSS and the samples subjected to simulated brazing cycles at temperatures of (*b*) 1053 K (780 °C), (*c*) 1073 K (800 °C), (*d*) 1093 K (820 °C), (*e*) 1123 K (850 °C), and (*f*) 1173 K (900 °C).

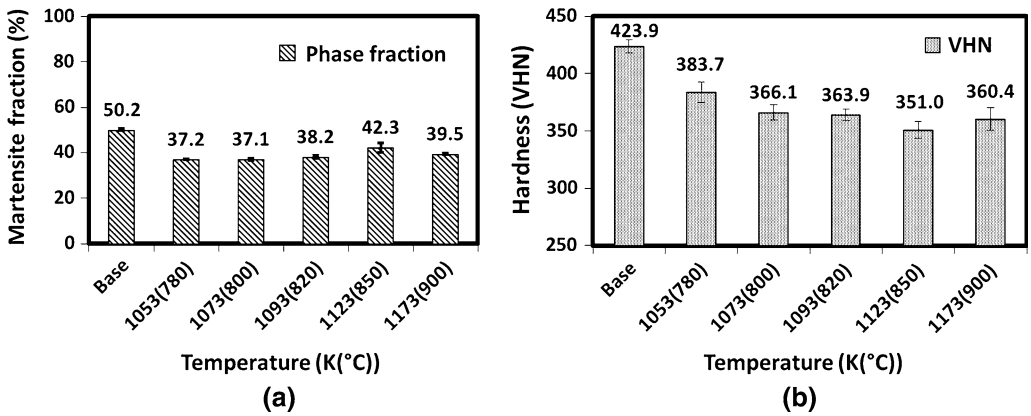

Fig. 4—Variation in (*a*) martensite phase fraction and (*b*) Vickers hardness of AMSS with temperature obtained in simulated brazing cycle.

looks to be well diffused. It can also be seen from Figures 6(a) through (f) that as the brazing temperature increased, the width of the BFM was reduced and defects such as voids or unfilled gaps were also reduced. Four different phases *viz*. silver solid solution denoted as α, copper solid solution denoted as β, Cu_3Sn

intermetallic, and Ni-Fe solid solution were encountered in the brazed joints of AMSS/pure silver, which are labeled in Figures 6(b), (d), and (f). The different phases were identified based on BSE contrast and EDS analysis. The α and β solid solutions as well as austenite and martensite are also identified by XRD analysis as presented in Figure 7. The Cu_3Sn phase could not be identified on XRD spectrum possibly due to its low volume fraction in the joints. Typical elemental compositions of different phases and their region of occurrence in the brazed joints are presented in Table II. Volume fraction of Cu_3Sn phase in BFM region was determined using point count method employed on BSE images. Calculated Cu_3Sn phase percentage was 0.65, 0.07, and 0 at brazing temperatures of 1053 K, 1073 K, and 1093 K (780 °C, 800 °C, and 820 °C), respectively. Thus, the Cu_3Sn phase was found to be absent at the brazing temperature of 1093 K (820 °C).

2. *Partitioning of Alloying Elements and Enhanced Wettability*

Another interesting feature observed at the interface on the steel side was the presence of Ni-Fe solid solution phase as shown in Figures 8(a) through (c). This phase was seen to exist not only as a continuous layer in contact with the steel but also as round-shaped particles surrounded by copper- or silver-rich matrix (see Figure 9(a)). The magnified image of one such Ni-Fe solid solution particle found at the interface is presented in Figure 9(b). The EDS line scan conducted across the particle is presented in Figure 9(c). It can be clearly seen from Figure 9(c) that the Ni-Fe particle is rich in iron and chromium at the center and in nickel toward the periphery. The matrix surrounding the particle is rich in copper and silver and lean in iron and chromium. This partitioning of the elements is consistent with the relative binary thermodynamic interactions observed between the elements. It is known that iron and copper have highly positive[24,27] enthalpy of mixing, whereas iron and nickel have negative enthalpy of mixing.[19,25] Copper and nickel have slightly positive enthalpy of mixing[24] but show complete miscibility. Thus, iron partitioned away from the copper-rich matrix, *i.e.*, toward the center and nickel-rich region separated the iron- and copper-rich regions. Chromium having slightly negative enthalpy of mixing with iron at lower concentrations and an extensive solubility in iron[28,29] tends to partition at the center along with iron. This partitioning phenomenon observed near the steel side of the interface also highlights the significance of nickel coating in enhancing the wettability of the BFM on the iron-rich steel. Poor wettability of Ag-Cu based BFM on iron-rich steel was also because of the highly positive enthalpy of mixing between these elements. However, nickel acts as a good separator and helps in forming a good bond between the BFM and the steel.

The most interesting feature of the Ni-Fe phase is the segregation of iron and chromium at the center of these particles. Given the fact that only nickel was in direct contact with the BFM at the beginning of the brazing, one of the hypotheses for this may be that iron and chromium started to diffuse into nickel coating during brazing and the Ni-Fe particles were then separated from the bulk to dissolve into the liquid braze metal. Now, since iron wants to move away from copper or silver in the BFM on account of its positive enthalpy of mixing with them, it tended to segregate at the center of the particle and nickel diffused toward the surface of the particle. Chromium, being likened by iron, diffused along with iron toward the center of the particle. In this process, iron, chromium, and nickel were clearly seen to manifest the phenomenon of uphill diffusion. This phenomenon can be used to explain the mechanism of forming good bond between the silver-rich BFM and the iron-rich steel in the presence of the intermediate nickel coating.

3. *Concentration Profiles Across the Brazed Joints*

Figure 10(a) presents the BSE micrograph of the joint prepared at 1093 K (820 °C) and the dotted line on the micrograph shows the line across which the concentration profiles were obtained with point-by-point analysis with EPMA. The concentration profiles obtained by EPMA are presented in Figure 10(b). From EPMA profiles developed, the whole braze joint can be considered to consist of four regions, which are AMSS, interface and BFM, diffusion-assisted zone (DAZ) and pure silver, which are identified in Figure 10(a). The interface and BFM region consists of multiple phases. On the silver side of the joint, smooth concentration gradients of copper and silver are evident in all joints. Thus, a good DAZ has developed at the silver-BFM interface. Figure 10(c) shows the silver-rich side of the ternary Ag-Cu-Sn isotherm at 1093 K (820 °C) as obtained by using thermodynamic software Thermocalc. The sequence of compositions developed at the BFM/Silver interface is also plotted on the isotherm as circles.

Similar EPMA profiles were also obtained on the joints prepared at brazing temperatures of 1053 K and 1073 K (780 °C and 800 °C), which are presented in Figures 11(a) and (b). The profiles were used to measure the widths of various regions in the joint as a function of brazing temperature and the data are presented in Figure 12. Width of the DAZ region was found to increase with increasing brazing temperature, whereas that of BFM was found to decrease. Thus, higher temperature was found to be beneficial for developing better DAZ and so, better bonding.

4. *Microstructure Evolution in the Brazed Joints*

From the microstructural and elemental analysis presented above and from the sequence of compositions plotted on the Ag-Cu-Sn ternary isotherm presented in Figure 10(c), following steps can be hypothesized to occur in the evolution of microstructure across the brazed joints of nickel-coated AMSS steel and pure silver.

1. On the AMSS side of the interface, the interdiffusion between nickel coating and steel starts during the heating stage. The iron and chromium from AMSS side diffuse into nickel and nickel diffuses in the opposite direction. The interdiffusion continues

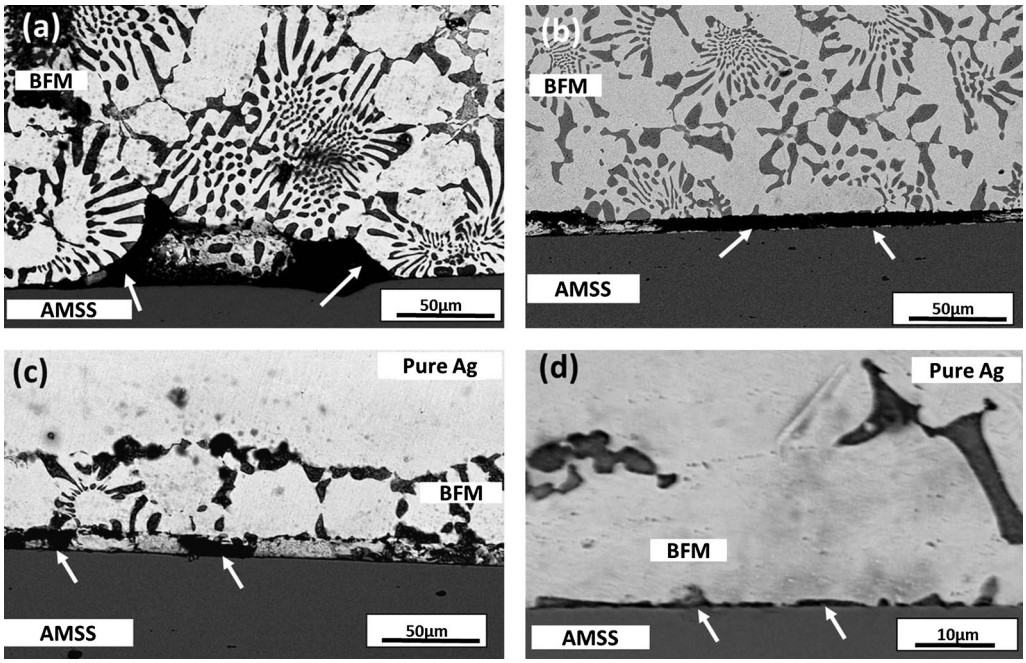

Fig. 5—Micrographs of brazed joint with AMSS used without nickel coating. (*a*, *b*) are AMSS/AMSS at 1058 K and 1093 K (785 °C and 820 °C), respectively. (*c*, *d*) are for AMSS/pure Silver at 1058 K and 1093 K (785 °C and 820 °C), respectively. The arrows indicate the unfilled gaps or voids at the interfaces.

during brazing too and it forms an iron-diffused nickel layer, which also contains some chromium. To confirm this, a set of Ni-coated AMSS placed in contact with BFM was heated to 1013 K (740 °C) (to avoid start of melting of the BFM) and cooled down from that temperature. The interface developed in this experiment is presented in Figure 13(a). EDS line scan was performed across this interface and the concentration profiles so obtained for iron, nickel, chromium, copper, and silver are presented in Figure 13(b). The hypothesis is confirmed from the concentration gradients developed for various elements at the AMSS/BFM interface. Interestingly, it was also noted that copper from the BFM too starts diffusing into nickel coating during heating up, which is reflected in building up of copper concentration in the nickel coating region as shown in Figure 13(b).

2. At the brazing temperature, BFM melts and starts to interact with both AMSS and pure silver. The BFM liquid wets well over the steel surface due to the presence of nickel coating. During the interaction, iron-diffused nickel coating starts dissolving into the melt. The elemental partitioning occurs in the Ni-Fe particles as discussed earlier. Thus, at the steel interface, a small diffusion layer forms between the iron-diffused nickel coating and the BFM along with detached Ni-Fe particles, which are finely dispersed in the Ag-Cu rich matrix.
3. Simultaneously, liquid BFM interacts with pure silver side and silver diffuses from pure silver into the liquid BFM, whereas copper and tin diffuse into the pure silver. The composition sequence observed in Figure 10(c) indicates that as more and more silver diffuses into the liquid BFM, the solid fraction increases, *i.e.,* the BFM continues solidifying from silver-rich side toward the BFM side. At the same time, copper and tin diffuse into pure silver yielding a good diffusion-assisted zone, which is beneficial for a strong bond.
4. The last liquid solidified would be at the center of the joint, which is evident from the eutectic Cu_3Sn phase observed in the central portion of the joints; see Figures 7(a) and (b). This also leads to shrinkage porosity observed at the center of the joints, especially at lower temperatures of brazing. At the higher temperature of 1093 K (820 °C), the better diffusion of alloying elements toward the center of the joint and the higher fluidity of the liquid BFM may have assisted in avoiding the pore formation at the center. The increased diffusivities of the elements at higher temperature of 1093 K (820 °C) possibly helped better distribution of the alloying elements in the solid solution phases. Moreover, diffusion of silver from pure silver into the BFM melt made the original BFM composition richer in silver and dilute in copper and tin. This is also evident from the increasing thickness of DAZ and decreasing width of BFM with brazing temperature as shown in Figure 12. This may have helped in eliminating the occurrence of Cu_3Sn phase in samples brazed at higher temperature of 1093 K (820 °C).

5. *Hardness Profiles Across the Joint*

Figure 14 shows the variation of hardness values across the brazed joints of AMSS/pure silver at three different brazing temperatures. As the indenter traversed from AMSS to pure Silver, no significant variations in

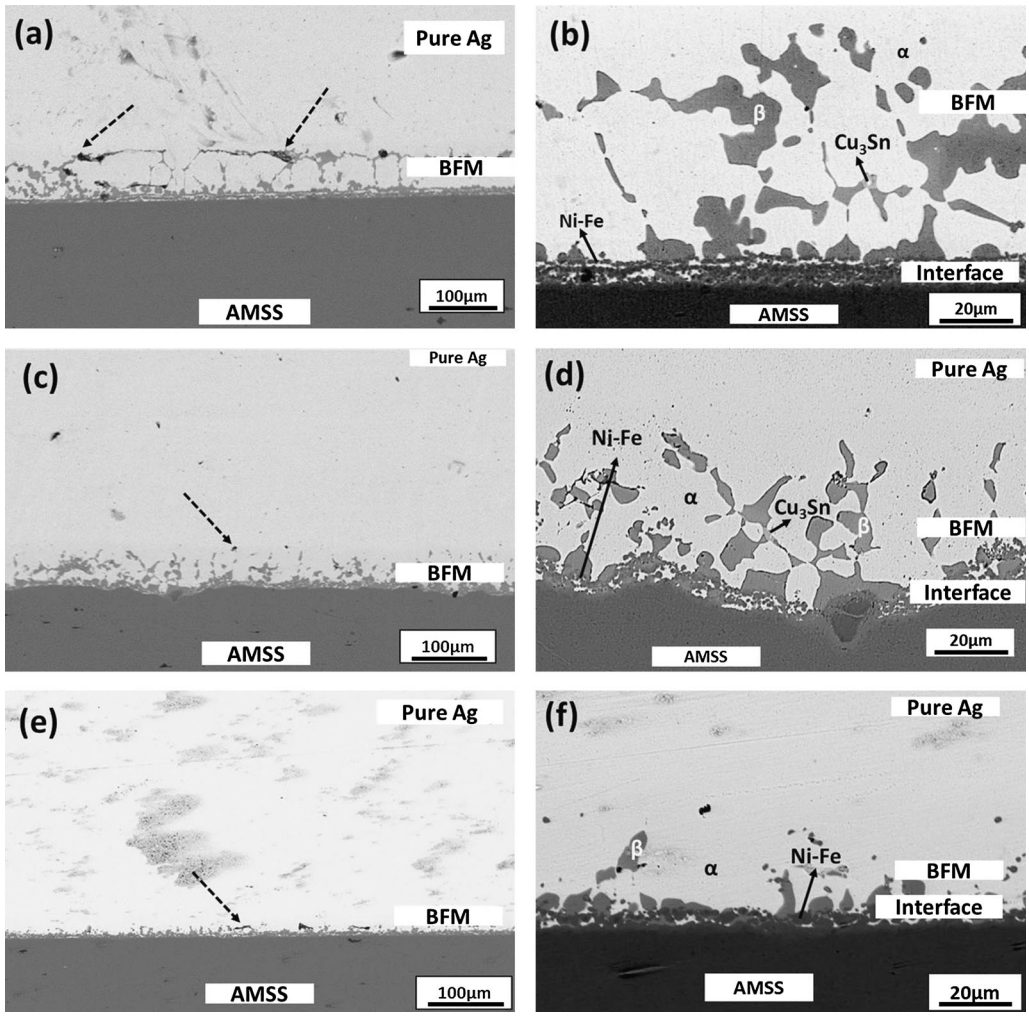

Fig. 6—BSE images of joints of AMSS to pure Silver brazed at (*a*, *b*) 1053 K (780 °C) (*c*, *d*) 1073 K (800 °C), and (*e*, *f*) 1093 K (820 °C). The dashed arrows point to the voids present in the joint and solid arrows show the indicated phases.

hardness values were observed within the base material AMSS. However, the hardness values drastically reduced in the brazed joint. This is applicable for all brazing temperatures studied. As expected, hardness of AMSS is greater than pure silver and the hardness across the joint was found to be in between that of the two base materials. Dotted line in each graph shows the base AMSS's hardness. Reduction in hardness values of AMSS was observed after brazing.

In order to enhance the properties of the base material affected due to the brazing process, a sub-zero treatment was conducted on the brazed joint, which consisted of immersing the joint in a liquid nitrogen for 0.5 and 2.5 hours. The hardness values of the AMSS at the interface before and after the post-brazing sub-zero treatments are presented and compared with the base material hardness away from the interface in Figure 15. It can be seen from Figure 15 that the hardness of the base material was recovered after a sub-zero treatment of 2.5 hours due to the martensitic transformation. Thus, a sub-zero treatment is recommended after the brazing cycle for recovering the strength of the base material.

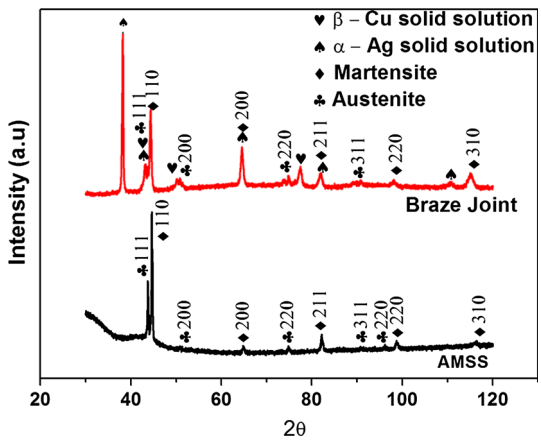

Fig. 7—XRD spectra of the base AMSS and the brazed joint prepared at 1073 K (800 °C).

6. *Lap shear Strength of the Joint*

To understand the relative strengths of the brazed joints, lap shear tests were carried out on the joints. Initially, tests were carried out on AMSS/pure

Table II. Elemental Distribution (at pct) in Each Phase and Its Region of Occurrence in AMSS/Pure Silver Joints

Phases	Region	Ag	Cu	Sn	Fe	Cr	Ni
α- White color	BFM and Interface	85.9	12.3	1.5	0.00	0.1	0.1
β- Dark color	BFM and Interface	2.2	87.6	2.2	1.8	0.2	5.9
Cu_3Sn—Gray color	BFM	7.9	71.3	17.8	0.2	0.00	2.7
Ni-Fe Solid Solution	Interface between BFM and AMSS	2.7	12.4	0.5	31.9	6.4	46.0

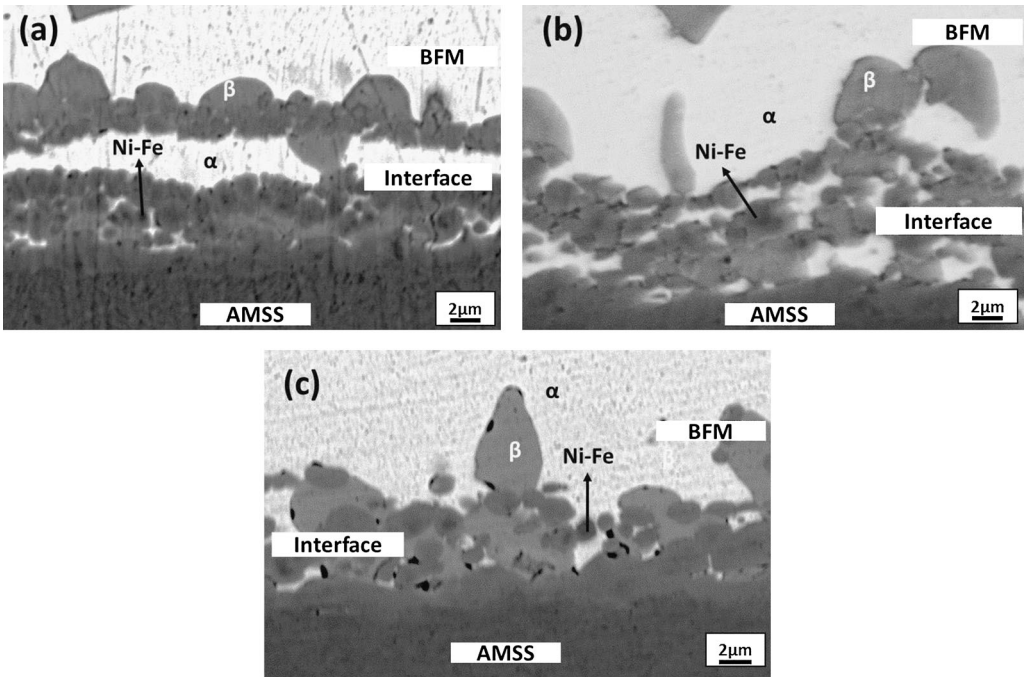

Fig. 8—BSE micrographs of the interface on steel side of the AMSS/pure silver joint brazed at (*a*) 1053 K (780 °C) (*b*) 1073 K (800 °C), and (*c*) 1093 K (820 °C).

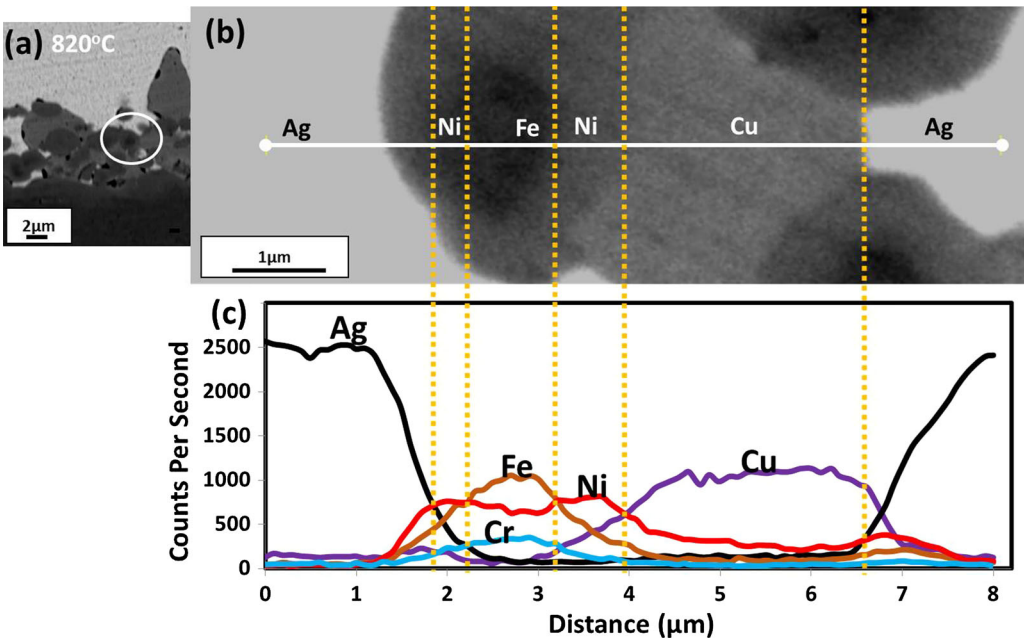

Fig. 9—(*a*) BSE micrograph of the interface of the brazed joint on the steel side at 1093 K (820 °C), (*b*) Zoomed-in Ni-Fe phase, where the EDS line profile was captured and (*c*) EDS line profile across Ni-Fe phase.

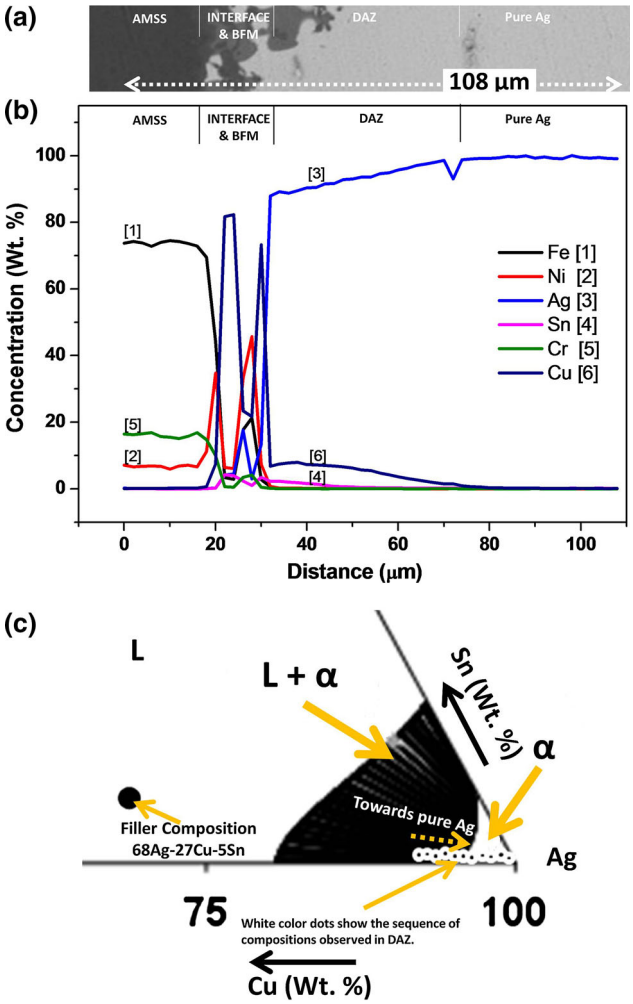

Fig. 10—(*a*) Microstructure of AMSS/pure silver-brazed joint at 1093 K (820 °C) (dotted line shows where EPMA scan was done), (*b*) EPMA profile and (*c*) Silver-rich side of the ternary Ag-Cu-Sn isotherm at 1093 K (820 °C) with the compositions appearing on the silver side of the joint plotted on the isotherm as white circles.

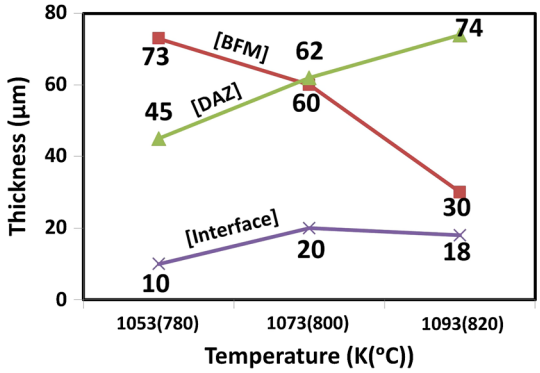

Fig. 12—Thickness of various regions of AMSS/pure silver-brazed joints at different temperatures.

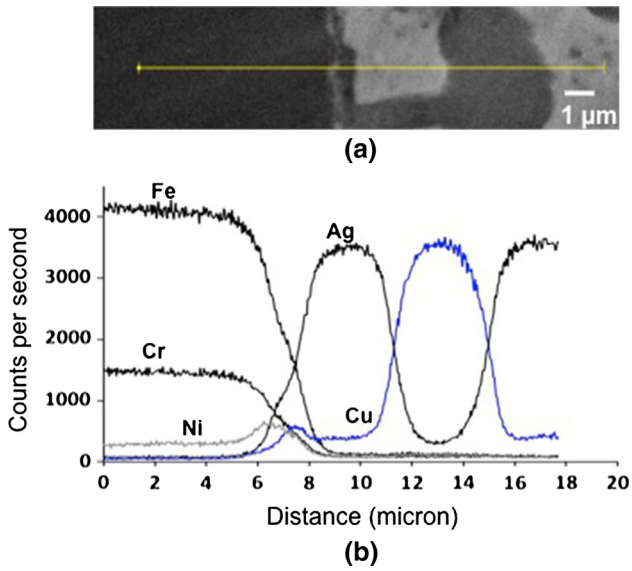

Fig. 13—(*a*) BSE image of the AMSS/BFM interface that was heated to 1013 K (740 °C) and cooled down and (*b*) Concentration profiles obtained by EDS line scan done across the interface shown in (a).

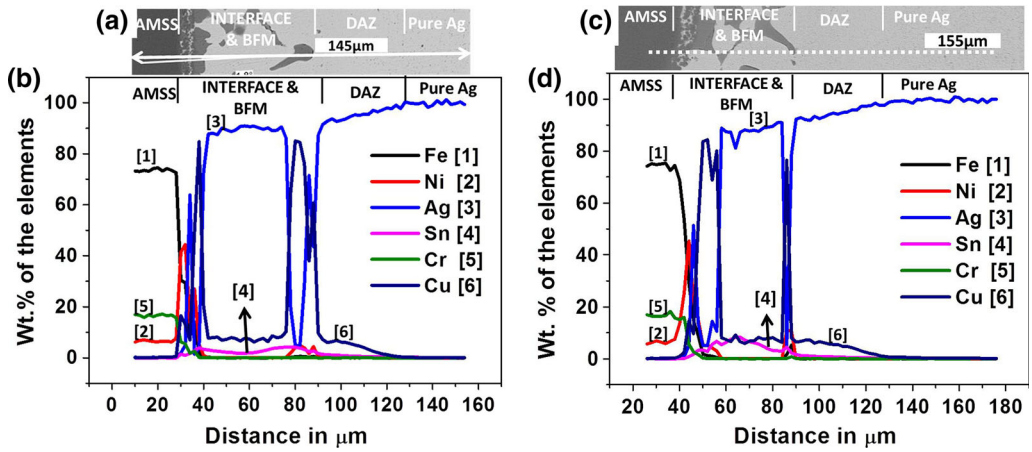

Fig. 11—(*a*, *c*) Microstructures of AMSS/pure silver braze joint at 1073 K (800 °C) and 1053 K (780 °C) (dotted lines show where EPMA scans were done) (*b*, *d*) EPMA profiles of AMSS/pure silver braze joint at 1073 K (800 °C) and 1053 K (780 °C).

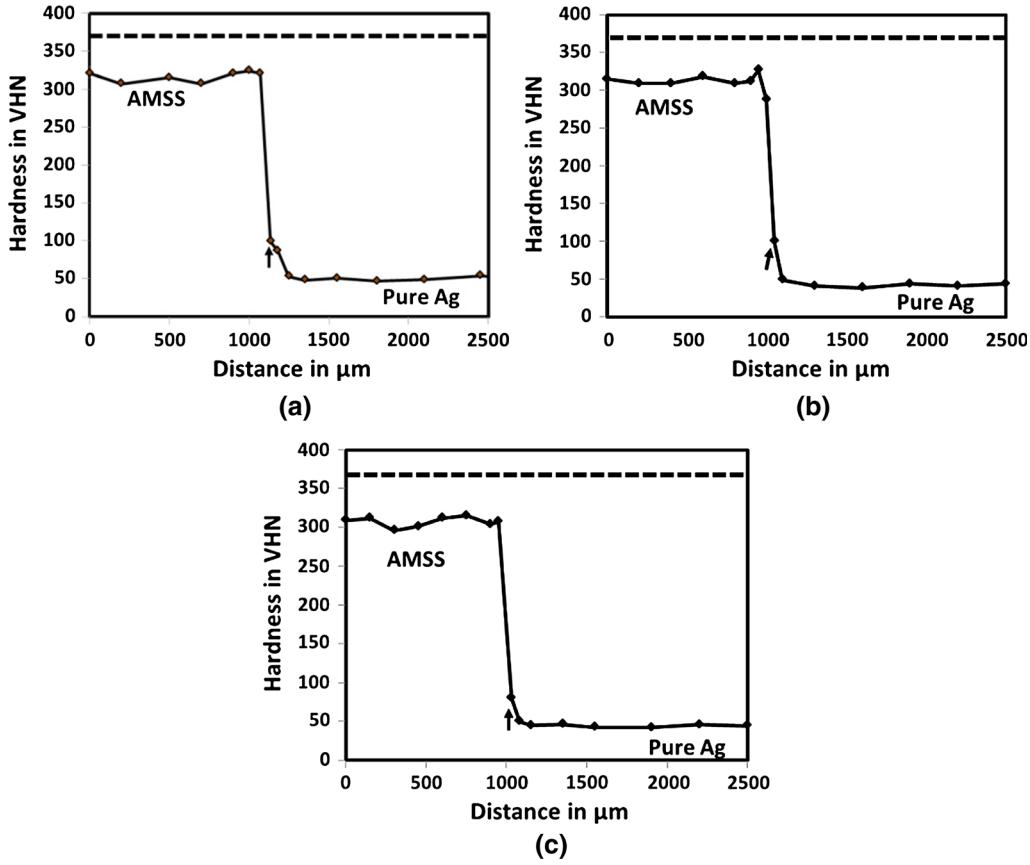

Fig. 14—Hardness profiles of the AMSS/pure silver-brazed joints fabricated at (*a*) 1053 K (780 °C), (*b*) 1073 K (800 °C), and (*c*) 1093 K (820 °C). Dotted line and arrow marks in each graph show the base AMSS hardness and the location of AMSS/BFM interface, respectively.

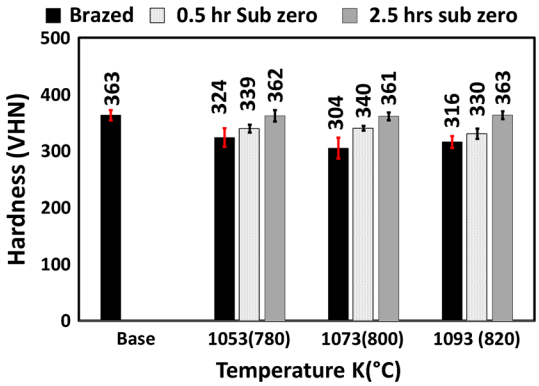

Fig. 15—Comparison of hardness values of base AMSS with heat-affected AMSS in the as-brazed and sub-zero-treated samples.

silver-brazed joint with 3T configuration (T is the thickness of the substrate) and failure was observed on the silver side with breaking load of 5-6.5 kN for three samples tested. Further lap shear samples were prepared with AMSS/pure silver joints with 1T configuration, at 1093 K (820 °C) alone. The observed failure in 1T was at pure silver base metal near to lap area with breaking load of 5.2-6 kN for 3 samples tested. In order to understand the relative joint strengths, the subsequent lap shear samples were prepared with joints of AMSS to AMSS at three different temperatures of 1053 K, 1073 K, and 1093 K (780 °C, 800 °C, and 820 °C). The obtained lap shear strength values were 120 ± 7 MPa, 119 ± 12 MPa, and 134 ± 4.5 MPa for the joints prepared at 1053 K (780 °C), 1073 K (800 °C), and 1093 K (820 °C), respectively. Failure locations in all these cases were at the braze joints. It should be noted that the above-mentioned lap shear strengths are not a true indication of the bonding strength between AMSS and pure silver and should be taken only for relative assessment of the joints prepared at different temperatures. Thus, the brazed joint prepared at 1093 K (820 °C) was found to be the strongest among the three temperatures studied. This is possibly because of the lowest defect density and the largest diffusion-assisted zone in these samples.

IV. SUMMARY

Based upon the results and analysis presented, the important findings can be summarized as follows:

- Based on the results of DSC analysis and observed fluidity of the liquid BFM, the brazing of AMSS steel and pure silver was conducted at the temperatures of 1053 K, 1073 K, and 1093 K (780 °C, 800 °C, and 820 °C).
- The BFM was observed to have poor wettability on the bare surface of AMSS steel. Hence, nickel coating was deposited on AMSS surface before

brazing. The nickel coating was observed to enhance the wettability of the BFM on the steel, giving good metallurgical bonding. The partitioning of iron, chromium, and nickel was observed in the Ni-Fe solid solution particles to take place through uphill diffusion. Thus, the thermodynamic and diffusional interactions were observed to play a significant roll in enhancing the metallurgical bonding of the Ag-Cu-Sn-based BFM with the nickel-coated steel.

- No continuous layer of intermetallic was found to form at any interface in these joints at any brazing temperature.
- Small fraction of intermetallic particles were observed at the center of the joints prepared at 1053 K and 1073 K (780 °C and 800 °C). No intermetallics were observed in the joints formed at 1093 K (820 °C).
- At brazing temperature of 1093 K (820 °C), brazed joints of AMSS with pure silver showed good flowability of liquid BFM with less defects and the absence of Cu_3Sn intermetallic phase. Also, the DAZ on the silver side was larger in joints made at 1093 K (820 °C). This also reflected in the higher lap shear strength of the joints prepared at 1093 K (820 °C) compared to the other two temperatures. Hence, the brazing temperature of 1093 K (820 °C) is recommended. A post-brazing sub-zero treatment was necessary to recover the properties of the base AMSS steel near the joint regions.

V. ACKNOWLEDGMENTS

Vikram Sarabhai Space Centre (VSSC), Thiruvananthapuram is acknowledged for financially supporting this work. Space Technology Cell at IIT Kanpur (IITK-STC) is also acknowledged for their support. Mr. Siva Kumar and Pradeep from ACMS, IIT Kanpur are acknowledged for facilitating use of SEM and EPMA facilities. Thanks are also due to Prof. N. P. Sudharshana from Department of Humanities and Social Sciences at IIT Kanpur for reviewing the manuscript for its English.

REFERENCES

1. N.M. Voznesenskaya, E.N. Kablov, A.F. Petrakov, and A.B. Shal'kevich: *Met. Sci. Heat Treat*., 2002, vol. 44, pp. 300–303.
2. J. Li, Y. He, D. Xiong, Y. Qin, J. Chen, and H. Zhu: *Tribol. Int.,* 2016, vol. 100, pp. 178–85.
3. A.A. Voevodin, C. Muratore, and S.M. Aouadi: *Surf. Coat. Technol*, 2014, vol. 257, pp. 247–65.
4. A. Erdemir: *Tribol. Int*., 2005, vol. 38 (3), pp. 249–56.
5. Evren. Atasoy and Nizamettin. Kahraman: *Mater. Charact*., 2008, vol. 59, pp. 1481–90.
6. Y.Q. Deng, G.M. Sheng, Z.H. Huang, and L.Z. Fan: *Sci. Technol. Weld. Join*., 2013, vol. 18, pp. 143–46.
7. L.J. Swartzendruber: *J. Phase Equilib*., 1984, vol. 5, pp. 560–64.
8. A. Khorram, M. Ghoreishi, M.J. Torkamany, and M.M. Bali: *Opt. Laser Technol*., 2014, vol. 5, pp. 560–64.
9. K. Nagatsuka, Y. Sechi, Y. Miyamoto, and K. Nakata: *Mater. Sci. Eng. B*, 2012, vol. 177, pp. 520–23.
10. D.K. Basri, L. Sisamouth, Y. Farazila, Y. Miyazawa, and T. Ariga: *Mater. Res. Innov*., 2014, vol. 18 (6), pp. 429–32.
11. D.L. Olson: *ASM handbook: Welding, Brazing, and Soldering*, ASM International, Materials Park, OH, 1993.
12. G. Humpston and D.M. Jacobson: *Principles of Brazing*, ASM International, Materials Park, OH, 2005.
13. V.P. Solntsev, B.S. Yermakov, and O.L. Sleptsov, *Mater. Low Cryog. Temp*., ISBN 978-5-93808 157 4.
14. Ya.M. Potak, V.V. Sachkov, and L.S. Popova: *Met. Sci. Heat Treat*., 1960, vol. 2, pp. 273–78.
15. V.I. Novikov, V.V. Dmitriev, and K.I. Nedashkovskii: *Met. Sci. Heat Treat*., 2014, vol. 56 (3-4), pp. 159–64.
16. V.I. Novikov, V.N. Semenov, and V.V. Dmitriev: *Met. Sci. Heat Treat*., 2001, vol. 43 (11-12), pp. 481–83.
17. R.D.K. Misra, V.S.A. Challa, P.K.C. Venkatsurya, Y.F. Shen, M.C. Somani, and L.P. Karjalainen: *Acta Mater*., 2015, vol. 84, pp. 339–48.
18. S. Srikanth, P. Saravanan, V. Kumar, D. Saravanan, L. Sivakumar, S. Sisodia, K. Ravi, and B.K. Jha: *Int. J. Metall. Eng*., 2013, vol. 2 (2), pp. 203–13.
19. R. Boom, F.R. DeBoer, A.K. Niessen, and A.R. Miedemma: *Physica*, 1983, vol. 115B, pp. 285–309.
20. E Ma, J-H He, and PJ Schilling: *Phys. Rev. B*, 1997, vol. 55 (9), pp. 5542–45.
21. O. Kozlova, R. Voytovych, M.-F. Devismes, and N. Eustathopoulos: *Mater. Sci. Eng. A*, 2008, vol. 495, pp. 96–101.
22. N. Eustathopoulos, M.G. Nicholas and B. Drevet: *Wettability at High Temperatures*, 1st edn. Pergamon Materials Series, vol. 3, Elsevier Science Ltd., Oxford, UK, 1999, pp. 193–97.
23. R.M. Do Nascimento, A.E. Martinelli, and A.J.A. Buschinelli: *Cerâmica*, 2003, vol. 49, pp. 178–98.
24. M.A. Turchanin and P.G. Agraval: *Powder Metall. Met. Ceram*., 2008, vol. 47 (1-2), pp. 26–39.
25. W. Rammensee and G. Donald: Fraser: *Berichte der Bunsengesellschaft für PhysikalischeChemie*, 1981, vol. 85, pp. 588–92.
26. F. M. Hosking, J. J. Stephens and J. A. Rejent, Welding Journal-New York, 1999, pp. 127-s.
27. J.Z. Jiang, C. Gente, and R. Bormann: *Mater. Sci. Eng. A*, 1998, vol. 242 (1), pp. 268–77.
28. T. P. Klaver, C. T. P., R. Drautz, and M. W. Finnis, *Phys. Rev. B*, 2006, vol. 74(9), pp. 94435.
29. W. Xiong, M. Selleby, Q. Chen, J. Odqvist, and Y. Du: *Crit. Rev. Solid State Mater. Sci*., 2010, vol. 35, pp. 125–52.